Proc. 13th Int. Conf. on Nucleus-Nucleus Collisions
JPS Conf. Proc. **32**, 010091 (2020)
https://doi.org/10.7566/JPSCP.32.010091

Precise Measurements of the Mass and the Binding Energy (B_Λ) of the Hypertriton at $\sqrt{s_{NN}}$ = 200 GeV with the Heavy Flavor Tracker at RHIC-STAR

Peng Liu[1,2,3] (for the STAR Collaboration)

[1]*Shanghai Institute of Applied Physics, Chinese Academy of Sciences, Shanghai 201800, China*
[2]*University of Chinese Academy of Sciences, Beijing 100049, China*
[3]*Brookhaven National Laboratory, Upton, New York 11973, USA*

E-mail: pengliu@rcf.rhic.bnl.gov

(Received July 21, 2019)

The excellent invariant mass distributions of hypertriton and antihypertriton are reconstructed via its 2-body and 3-body mesonic decay channels using the high statistics data of Au+Au collisions at $\sqrt{s_{NN}}$ = 200 GeV collected by the STAR experiment in 2014 and 2016. The invariant mass distributions are almost combinatorial background free benefitting from the high precision tracking system of the Heavy Flavor Tracker, and the great particle identification of the Time Projection Chamber and Time-Of-Flight detector in the STAR experiment. These data allow us to precisely determine the hypertriton mass and its binding energy.

KEYWORDS: Hypertriton mass, Binding energy, Heavy Flavor Tracker, Heavy-Ion Collisions

1. Introduction

Recent astrophysics observations of the neutron stars, such as a star with the mass that is 2.2 of the solar mass measured using relativistic Shapiro delay in 2019 [1] and a star with radius about 11 km measured using gravitational waves from a neutron star merging in 2018 [2], challenge our understanding of the hyperon role in neutron stars (the so-called "hyperon puzzle" [3, 4]). Repulsive Hyperon-Nucleon (YN) and Hyperon-Hyperon (YY) interactions have been considered as an alternative solution for this hyperon puzzle by astrophysicists [5]. The hyperon-nucleon or hyperon-hyperon scattering experiments would be an ideal tool to study the properties of YN and YY interactions. However, it is very difficult to obtain a stable hyperon beam to perform the scattering experiments due to the very short lifetime of hyperon. To date, the YN and YY scattering data are very poor. The hypertriton ($^3_\Lambda$H) as the lightest hypernucleus (a kind of nuclei in which at least one hyperon is bounded) yet discovered is made up of a proton, a neutron, and a hyperon (Λ). It is a natural hyperon-nucleon-nucleon (YNN) interacting system and thus its fundamental properties, such as the lifetime and mass are directly connected to the properties of YNN interaction [6, 7]. Fortunately, abundant $^3_\Lambda$H is produced in high-energy nucleus-nucleus collisions [6–11]. Therefore, the $^3_\Lambda$H can serve as an excellent experimental way to explore the YN interaction. Recent precise lifetime measurements of $^3_\Lambda$H had been carried out in heavy-ion collisions [7, 12, 13], but the most precise measurements of the mass were made about 40 years ago [14–18] and they may suffer from a large systematic uncertainty [18, 19]. The STAR detector [20–22] (the Solenoidal Tracker at RHIC) located in Brookhaven National Laboratory provides us an ideal playground to precisely measure the masses of $^3_\Lambda$H and its antimatter partner $^3_{\bar{\Lambda}}\overline{\mathrm{H}}$ [10]. This proceeding presents the analysis details including detector configuration, particle identification, topology cuts, and the preliminary results of precise measurement of $^3_\Lambda$H and $^3_{\bar{\Lambda}}\overline{\mathrm{H}}$ using the STAR detector.

2. Analysis Details

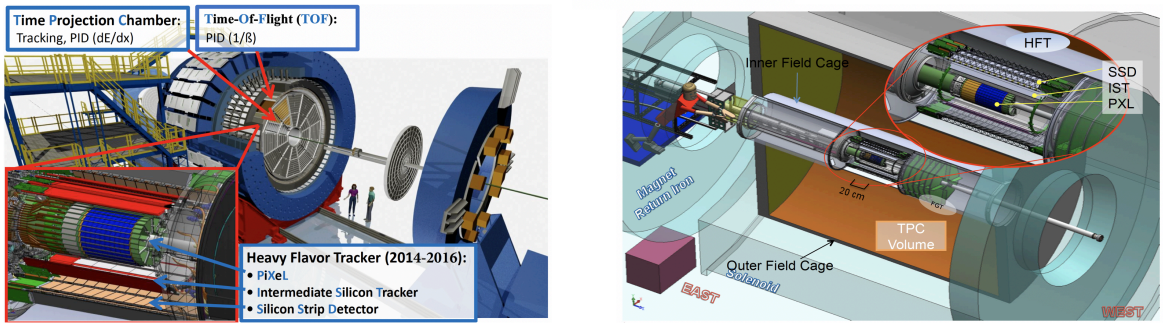

Fig. 1. The view of the STAR detector and its subsystems. Left plot shows full view of STAR. The TPC and TOF detectors are used for charged particle identification. The HFT and TPC detectors are used for the high precision tracking. The magnified component is HFT. The right plot shows the details of TPC and HFT. The HFT has three subsystems installed in the center of TPC, namely PXL at the radii of 2.8 and 8 cm, IST at the radius of 14 cm, and SSD at the radius of 22 cm.

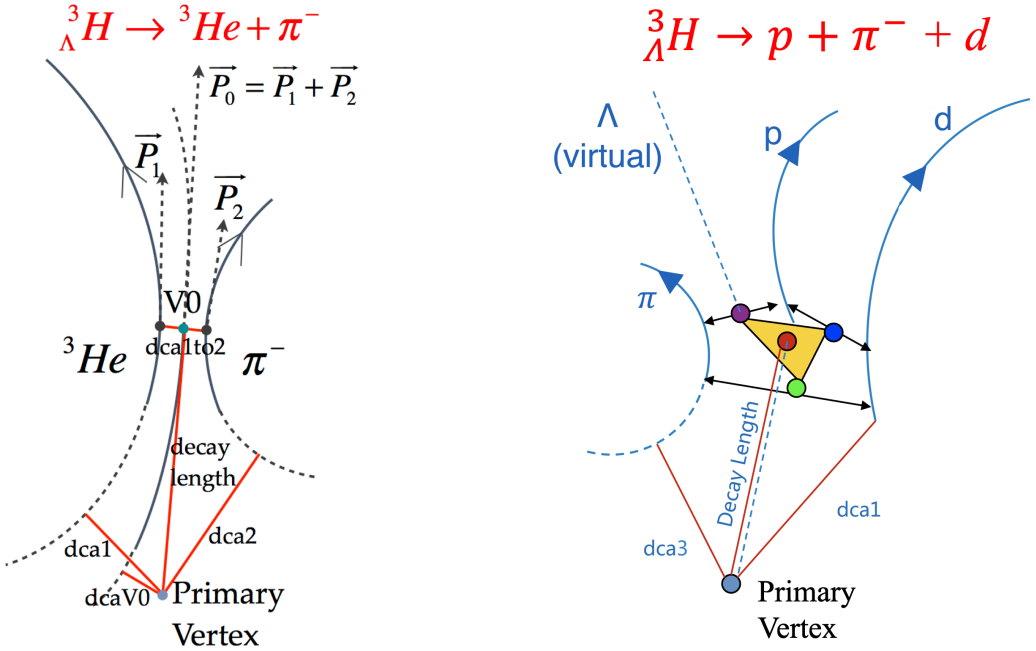

Fig. 2. The 2-body and 3-body hypertriton decay topologies. Primary vertex is the Au+Au collision vertex. The dca means the distance of closest approach (dca) between decay daughter's track and primary vertex. Decay vertex (V0) is defined as the middle point of closest approach between 2 decay daughters for 2-body decay (shown in left plot). For 3-body decay, the decay vertex (red point) is the middle point of the triangle formed by the violet, green, and blue points. The three points (violet, green, and blue) are the middle points of closest approach between each 2 decay daughter's tracks (shown in right plot). Decay length is the distance between reconstructed decay vertex and primary vertex.

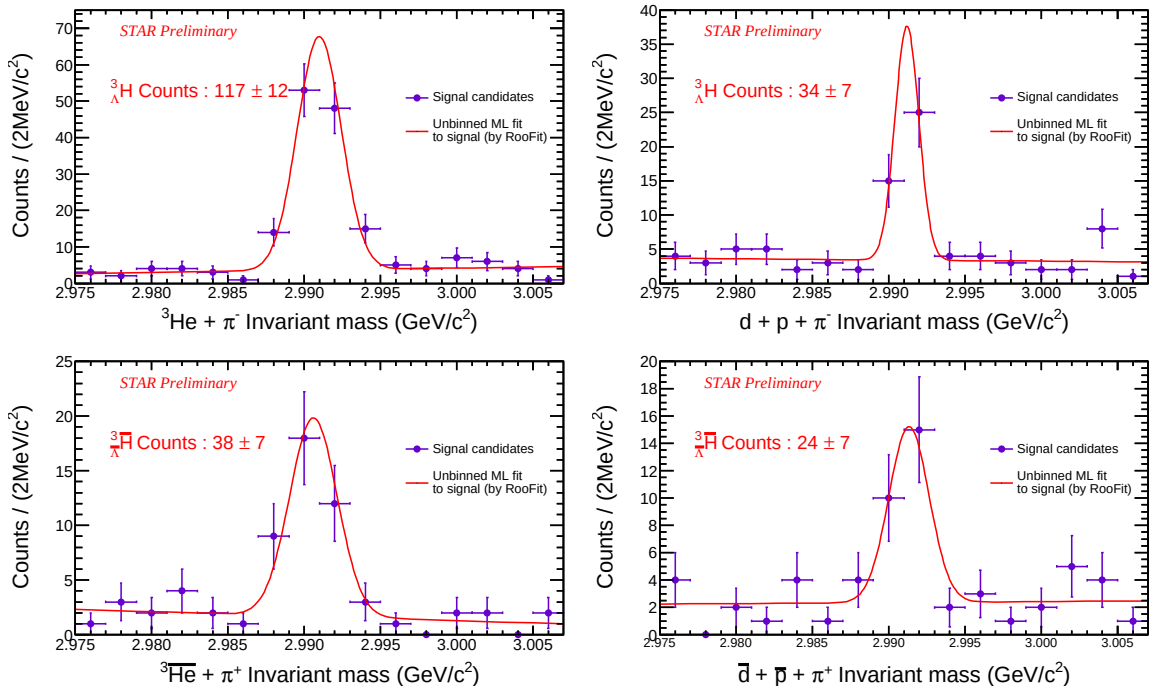

Fig. 3. Invariant mass distributions of ${}^{3}_{\Lambda}\text{H}$ and ${}^{3}_{\bar{\Lambda}}\overline{\text{H}}$ reconstructed through its 2-body and 3-body mesonic decay channels. The data points are the raw counts with only statistical errors. Red curves show the fitting results using unbinned Maximum Likelihood (ML) fit method with the Gaussian function to describe a signal and the first-order polynomial function to describe the background.

The invariant masses of ${}^{3}_{\Lambda}\text{H}$ and ${}^{3}_{\bar{\Lambda}}\overline{\text{H}}$ are reconstructed through its 2-body and 3-body mesonic decay channels ${}^{3}_{\Lambda}\text{H} \rightarrow {}^{3}\text{He} + \pi^-$ and ${}^{3}_{\Lambda}\text{H} \rightarrow \text{d} + \text{p} + \pi^-$ using the high statistics data collected in 2014 and 2016. About 1.2 billion events in 2014 and 3.3 billion events in 2016 are used in this analysis. The main detectors used in this measurement are the Time Projection Chamber [20] (TPC), Time-Of-Flight [22] (TOF) detector, and Heavy Flavor Tracker [21] (HFT) as shown in Fig. 1. Comparing the mean energy loss per unit of path length ($\langle dE/dx \rangle$) of charged particle in the TPC gas measured by TPC and speed (β) of particles measured by TOF with its expected values are used to identify the decay daughters. The HFT features an excellent spatial resolution better than 30 μm due to the good performance of its three subsystems: PiXeL (PXL), Intermediate Silicon Tracker (IST), and Silicon Strip Detector (SSD). The high spatial resolution of HFT in conjunction with TPC allow us to precisely determine the topology parameters as shown in Fig. 2. The topological cuts are used to suppress the background of reconstructed ${}^{3}_{\Lambda}\text{H}$ and ${}^{3}_{\bar{\Lambda}}\overline{\text{H}}$. For example, the distance of closest approach (dca) between the daughter track of the decayed particle and primary vertex is required to be larger than 0.010 cm and smaller than 3.0 cm for 2-body decay channel, while these values are required to be smaller than 3.0 cm, and larger than 0.010 cm for daughter deuteron, 0.015 cm for daughter proton, 0.020 cm for daughter π^- in the reconstruction via 3-body decay channel; the dca between each 2 daughters is required to be smaller than 0.020 cm; the decay length is required to be larger than 0.4 cm for 2-body decay channel and 0.6 cm for 3-body decay channel in 2014 data, and to be larger than 0.4 cm for 2-body decay channel and 0.8 cm for 3-body decay channel in 2016 data. After applying the optimized topology cuts mentioned above, the invariant mass distributions for ${}^{3}_{\Lambda}\text{H}$ and ${}^{3}_{\bar{\Lambda}}\overline{\text{H}}$ reconstructed via its 2-body and 3-body mesonic decay channels are shown in Fig. 3. In Fig. 3, the red curves are the fitting results using unbinned Maximum Likelihood (ML) fit method

with the Gaussian function to describe a signal and the first-order polynomial function to describe the background. The reconstructed candidates of ${}^{3}_{\Lambda}\mathrm{H}$ and ${}^{3}_{\bar{\Lambda}}\overline{\mathrm{H}}$ are 117 ± 12 and 38 ± 7 for the 2-body decay channel, 34 ± 7 and 24 ± 7 for the 3-body decay channel. The numbers of candidates of ${}^{3}_{\Lambda}\mathrm{H}$ and ${}^{3}_{\bar{\Lambda}}\overline{\mathrm{H}}$ are calculated from the counts in signal region of invariant mass distributions shown in Fig. 3 and the backgrounds are estimated by side bands.

3. Summary

The invariant mass distributions of ${}^{3}_{\Lambda}\mathrm{H}$ and ${}^{3}_{\bar{\Lambda}}\overline{\mathrm{H}}$ are reconstructed via its 2-body and 3-body mesonic decay channels, ${}^{3}_{\Lambda}\mathrm{H} \rightarrow {}^{3}\mathrm{He} + \pi^{-}$ and ${}^{3}_{\Lambda}\mathrm{H} \rightarrow \mathrm{d} + \mathrm{p} + \pi^{-}$ using the Heavy Flavor Tracker in STAR at RHIC. The ${}^{3}_{\Lambda}\mathrm{H}$ and ${}^{3}_{\bar{\Lambda}}\overline{\mathrm{H}}$ candidates reconstructed through the 2-body decay channel are 117 ± 12 and 38 ± 7, respectively, and the candidates for the 3-body decay channel are 34 ± 7 and 24 ± 7, respectively. These data provide an opportunity to precisely measure the hypertriton lifetime and mass, which are directly related to the strength of the *YN* interaction. For more details see Ref. [23].

4. Acknowledgements

This work was supported in part by the China Scholarship Council under Contract No. 201704910615, the National Natural Science Foundation of China under Contract Nos. 11775288, 11421505, and 11520101004.

References

[1] H. T. Cromartie, *et al.*, Preprint at https://arxiv.org/abs/1904.06759 (2019).
[2] B. P. Abbott, *et al.* (The LIGO Scientific Collaboration and the Virgo Collaboration), Phys. Rev. Lett. **121**, 161101 (2018).
[3] D. Lonardoni, A. Lovato, S. Gandolfi, and F. Pederiva, Phys. Rev. Lett. **114**, 092301 (2015).
[4] J. L. Zdunik, and P. Haensel, Astron. Astrophys. **5**51, A61 (2013).
[5] M. Buballa, J. Phys. G: Nucl. Part. Phys. **41**, 123001 (2014).
[6] J. H. Chen, D. Keane, Y. G. Ma, A. H. Tang, and Z. B. Xu, Phys. Rep. **760**, 1-39 (2018).
[7] L. Adamczyk, *et al.* (STAR Collaboration). Phys. Rev. C **97**, 054909 (2018).
[8] S. Zhang, *et al.*, Phys. Lett. B **684**, 224-227 (2010).
[9] B. I. Abelev, *et al.* (STAR Collaboration), Science **328**, 58-62 (2010).
[10] P. Liu (for the STAR Collaboration), Nucl. Phys. A **982**, 811-814 (2019).
[11] P. Liu, J. H. Chen, Y. G. Ma, and S. Zhang, Nucl. Sci. Tech. **28**, 55 (2017).
[12] A. Gal, and H. Garcilazo, Phys. Lett. B **791**, 48-53 (2019).
[13] S. Acharya, *et al.* (ALICE Collaboration), Preprint at https://arxiv.org/abs/1907.06906 (2019).
[14] M. Juric, *et al.*, Nucl. Phys. B **52**, 1-30 (1973).
[15] G. Hohm, *et al.*, Nucl. Phys. B **4**, 511-526 (1968).
[16] W. Gajewski, *et al.*, Nucl. Phys. B **1**, 105-113 (1967).
[17] A. Gal, E. V. Hungerford, and D. J. Millener, Rev. Mod. Phys. **88**, 035004 (2016).
[18] P. Liu, J.-H. Chen, D. Keane, Z. Xu, and Y.-G. Ma, Preprint at https://arxiv.org/abs/1908.03134 (2019).
[19] P. Achenbach, S. Bleser, J. Pochodzalla, and M. Steinen, PoS **Hadron2017**, 207 (2018).
[20] M. Anderson, *et. al.*, Nucl. Inst. Methods Phys. Res. A **499**, 659-678 (2003).
[21] G. Contin, *et al.*, Nucl. Inst. Methods Phys. Res. A **907**, 60-80 (2018).
[22] W. J. Llope (for the STAR Collaboration), Nucl. Inst. Methods Phys. Res. A **661**, S110-S113 (2012).
[23] J. Adam, *et al.* (STAR Collaboration), Preprint at https://arxiv.org/abs/1904.10520 (2019).